THE AMERICAN SOCIETY OF MECHANICAL ENGINEERS
345 E. 47th St., New York, N.Y. 10017

96-GT-67

NUMERICAL SIMULATION OF SECONDARY FLOW IN GAS TURBINE DISC CAVITIES, INCLUDING CONJUGATE HEAT TRANSFER

Y.-H. Ho and M.M. Athavale
CFD Research Corporation, Huntsville, Alabama, USA

J.M. Forry
Allison Engine Co., Rolls Royce Aerospace Group,
Indianapolis, Indiana, USA

R.C. Hendricks and B.M. Steinetz
NASA Lewis Research Center,
Cleveland, Ohio, USA

ABSTRACT

A numerical study of the flow and heat transfer in secondary flow elements of the entire inner portion of the turbine section of the Allison T-56/501D engine is presented. The flow simulation included the interstage cavities, rim seals and associated main path flows, while the energy equation also included the solid parts of the turbine disc, rotor supports, and stator supports. Solutions of the energy equations in these problems usually face the difficulty in specifications of wall thermal boundary conditions. By solving the entire turbine section this difficulty is thus removed, and realistic thermal conditions are realized on all internal walls. The simulation was performed using SCISEAL, an advanced 2D/3D CFD code for predictions of fluid flows and forces in turbomachinery seals and secondary flow elements. The mass flow rates and gas temperatures at various seal locations were compared with the design data from Allison. Computed gas flow rates and temperatures in the rim and labyrinth seal show a fair to good comparison with the design calculations. The conjugate heat transfer analysis indicates temperature gradients in the stationary intercavity walls, as well as the rotating turbine discs. The thermal strains in the stationary wall may lead to altered interstage labyrinth seal clearances and affect the disc cavity flows. The temperature fields in the turbine discs also may lead to distortions that can alter the rim seal clearances. Such details of the flow and temperature fields are important in designs of the turbine sections to account for possible thermal distortions and their effects on the performance. The simulation shows that the present day CFD codes can provide the means to understand the complex flow field and thereby aid the design process.

INTRODUCTION

The demand for higher efficiencies in advanced gas turbine aero and aero-derivative engines has driven operating conditions to higher temperatures and pressures in compressor as well as in turbine sections. With increasing severity of conditions, management of the secondary flow system, which provides component cooling, has become increasingly important. The coolant flow is essential to keep components temperatures to acceptable levels to achieve long life cycles. The compressed coolant air also represents a loss of engine efficiency, and hence has to be minimized. In the modern gas turbine engine, secondary flow management is one of the most promising areas for engine efficiency increases and, hence, there is drive to minimize the coolant losses. Optimization of the secondary coolant systems in a gas turbine engine is important, and a thorough understanding of the flow and heat transfer processes that take place in the disc cavities in the turbine as well as in the compressor sections is essential. Effects of linking between the cavities and the main path must be taken into account when simulating these flows in the often interconnected disk cavities.

The flow and heat transfer processes in the single rim seal and disc cavity configurations have received a large amount of attention in the past. Early experimental and theoretical work considered simplified cavity and rim seal geometries to generate models for the performance of the cavities. Experimental and theoretical analyses of such configurations are given in References 1-3. A simple analytical model for disc cavity friction heating as well as main path gas ingestion was given by, *e.g.*, Hasser *et al.*[4]. These models were based on the integral momentum equations to treat the flow.

With the advent of the computational fluid dynamics (CFD) methodology, detailed analyses of the cavity flows were undertaken. Early CFD work was done on simplified geometries of a single disc cavity with the associated rim seal. Laminar and turbulent flows in such rotating cavities with inflow and outflow were presented by Chew[5,6]. More recently, Ko and Rhode[7] conducted studies on the heat transfer in a turbine disc with secondary cooling flows. Athavale *et al.*[8] also conducted a numerical study on a single cavity configuration, and variations in the cooling effectiveness in the cavity with purge flow and geometrical mismatches at the rim seal were investigated.

The majority of these studies on rim seal and disc cavity flows have concentrated on the single cavity-seal configuration with simplified cavity geometries. This approach provides a good first-order analysis, but it may not be satisfactory when applied to the

Presented at the International Gas Turbine and Aeroengine Congress & Exhibition
Birmingham, UK — June 10-13, 1996

flow problems in an actual engine. In an actual engine, the disc cavities have complex shapes, can have multiple connections with other cavities, and are connected to the main path flow. The interaction of secondary flow elements with other secondary flows and the main path can be quite strong, as illustrated in Hendricks *et al.*[9], and for this reason, the coupled intercavity and secondary-main path interaction needs to be explicitly included in the computations. This task has become easy with the current state-of-the-art multi-domain CFD codes, which allow the treatment of complicated shapes by domain splitting. A demonstration simulation of the interlinked cavities was given by Virr *et al.*[10]. Recently, Athavale *et al.*[11] presented a numerical study of the complete, complex secondary flow system in the UTRC Large Scale Rig.

The solid parts in a turbine often come into contact with gas streams with largely different temperatures. The thermal gradients set up in these parts need to be considered, as the resulting thermal strains can easily alter the tight seal clearances to a point where the cavity flows may produce unacceptable patterns. Given the trend for tighter seal clearances and reduced purge rates, these two items deserve more attention in order to produce cavity designs that generate acceptable efficiencies as well as component life. Recently, Athavale *et al.*[12] carried out the flow and conjugate heat transfer simulation of the Allison T-56 engine turbine disc cavities. They showed the effects of the labyrinth seal clearances on the flow characteristics as well as the possible thermal strains existing at the solid-fluid interfaces of the stator central support walls. In their predictions, three pairs of cavities were calculated separately. The flow simulation of the first pair of cavities did not include the conjugate heat transfer prediction and the rotor supports were not included in their study.

In this paper, a continuous and more thorough study was carried out on the turbine section of the Allison T-56 turboshaft engine to understand the flow and heat transfer processes that take place in the associated disc cavities. The entire turbine disc cavities, including three pairs of interstage cavities, were modeled. The conjugate heat transfer prediction included the inter-cavity walls that exist under the stator vanes and the rotor supports in between each pair of cavities. In addition, the walls that support the honeycomb rings that form stationary parts of the interstage labyrinth seals were also included in the simulation. In the present simulation the honeycombs were modeled as solid surfaces. The flow rates and gas temperatures at various seals were obtained and compared with the design data from Allison and the earlier prediction by Athavale *et al.*[12].

DESCRIPTION OF THE FLOW SOLVER

The numerical simulation was carried out with an advanced 2D/3D CFD code SCISEAL, developed for the analysis of fluid flows and forces in turbomachinery seals under a NASA contract[13]. Extensive validations of SCISEAL were performed over the past years. The flow fields inside look-through, stepped, plannar labyrinth seals were computed and compared to the experimental data (Przekwas et al.[14]). The effects of purge flow and rim seal geometry on the ingestion of main-flow gas into a generic turbine disc cavity were studied and the results were compared to the experimental data (Athavale et al.[15]). A finite-volume, pressure-based formulation is used to integrate the flow and scalar equations in a sequential manner. A modified version of the SIMPLEC procedure is used to link the pressure and velocities. The code can handle incompressible as well as low and high-speed compressible flows. An implicit multidomain capability is available and is extremely important in the present simulation, where the complex shapes of the cavities make single-block grid generation extremely difficult, if not impossible. The energy equation models both fluid and solid regions and the conjugate surfaces, and this feature is also important in the disc cavity analyses. A variety of turbulence models, including the standard and low-Re k-ε models and a two-layer k-ε models are available. High order spatial (up to 3rd) and temporal (2nd) discretization schemes can be used for the convective and time derivatives. Other relevant capabilities include variable gas properties and inclusion of the viscous dissipation in the energy equation.

FLOW CONFIGURATION

The configuration considered in this study consists of the three interstage pairs of disc cavities and the interstage labyrinth seals in the turbine section of the T56/501D engine of Allison Engine Company, Rolls Royce Aerospace Group. These engines are currently installed on the C-130 military transport planes. The characteristics of the T56/501D engine are: a pressure ratio of 14.1, a mass flow rate 15.7 kg/s, engine speed 14239 rpm. The engine delivers 5250 horse power at the sea level takeoff condition and the maximum turbine inlet temperature is 1364 K. The results presented in this paper are for the sea-level takeoff condition. Flow information inside the cavities was generated by Allison with their design codes and was made available for the comparison with the numerical results. The data include static pressures inside the cavities, and the flow rates and total temperatures of the gas at the rim and labyrinth seals. In this 2D, axisymmetric simulation, the ingestion effects due to rotor-stator interactions are neglected.

The complex geometry of the disk cavities was scanned directly from the engine drawings, and the outlines of the walls were generated and fed into a grid generation package. Several critical geometric parameters, such as the labyrinth seal clearances, the rim seal gaps, and the secondary flow injection areas were provided by Allison Engine Company. The flow field was assumed to be axisymmetric and, hence, a two-dimensional, multi-domain grid was built. The energy (temperature) solutions included the central walls under the stator vanes and the rotor supports between each pair of cavities. These walls and supports were also gridded for heat conduction in the solid portions. The total number of domains were 140, which had approximately 91,000 grid cells. For this calculation, a small initial effort was done to assess the grid independence of the solutions. It was found that no noticeable pressure changes were found compared to a coarser grid solution (Ref. 12). However, the effects of grid resolution on the flow details are still uncertain and require more grid dependency study. Further efforts are planned.

FLOW AND BOUNDARY CONDITIONS

At the upstream boundaries of the main paths (core flows) associated with the six rim seals, the inlet velocity and temperatures were specified, and constant static pressures were specified at the exit boundaries of each of these main paths. The inlet conditions differed at each of the main path section, and the values used here were established by the Allison design calculations. The mass flow rates and temperatures of the various purge flows were also known and were imposed at the appropriate locations in all the cavities. In the Stage 2-3 and 3-4 cavities, the purge flow locations were concentrated in double and single locations within the corresponding interstage seals, while the Stage 1-2 cavity block had several points of injection. The geometries of the turbine disc cavities and the interstage labyrinth seals as well as the locations of the purge flow injection are shown in Figure 1. Also shown in Figure 1 are the boundary conditions that were used in the

calculation.

In the simulation, walls on the left-hand side of the Stage 1-2 cavities as well as those underneath the Stage 1-2 cavities were assumed to be adiabatic due to a lack of temperature information at these locations. As mentioned above, the stationary walls under the stator vanes and the rotor supports were included in the energy equation computation. The surfaces of these walls were conjugate surfaces, and no explicit 'energy' boundary conditions were needed on these fluid-solid interfaces. The upper and lower boundaries of these supports were in contact with the hot main path gas and the cool secondary flows, and these walls were assumed isothermal (see Figure 1). The convective heat transfer effects at the top walls were ignored and average values of the main flow path gas temperatures were applied at these walls. All the other walls were also assumed isothermal, which essentially include all rotor walls. The temperatures of the cooling secondary flows were applied at these walls. For the momentum equations, all walls were no-slip walls, with appropriate tangential velocity conditions imposed on the stationary and rotating walls.

The two-dimensional, axisymmetric flow in the cavities and main path was assumed compressible with air as the working fluid. Sutherland's viscosity law was used to account for variations in the viscosity due to temperature. The central-differencing scheme (90%) was used for the convective fluxes in the momentum equations blending with a (10%) first-order upwinding damping. The turbulence in the flow was treated with the standard k-ε turbulence model with wall functions. Effects of viscous dissipation were included in the energy equation.

RESULTS AND DISCUSSION

The numerical results presented here are the streamline, static pressure and static temperature plots in each of the flow domains. The streamline plots are very useful in tracing the fluid motion; the static pressures contribute to a major portion of loading on solid surfaces; and, high static temperature gradients in the flow and solid parts may induce unacceptable thermal strains on the solid surfaces. Also presented below are the flow rates and temperatures at the rim and labyrinth seal locations, static pressure inside the Stages 2-3 and 3-4 cavities, and a comparison with the design data.

Stage 1-2 Cavities

In the stage 1-2 cavities, the design flow is at a labyrinth seal clearance of 0.3048 mm. There are several purge flow injection points, as well as a small exit path in the stator vanes as shown in Figure 1. The streamlines are plotted in Figure 2 and show evidence of the injection points. The left cavity has a large central recirculation bubble, which pushes the coolant flow up along the rotor wall and down along the stator wall, where one of the purge flow stream mixes with the cavity flow. A portion of the overall purge flow discharges through the left rim seal and a part through the upper path in the stator vane (path 5 in Figure 1). The remaining flow passes on through the labyrinth seal into the right cavity. This cavity also has a large recirculation bubble that entrains this coolant flow and eventually is exhausted into the main path through the right rim seal. The flow patterns in both the rim seals indicate unidirectional flow out to the main stream and no ingestion of the hot gas. This is reflected in the temperature plot, Figure 4, where the bulk of the flow is relatively cool. The conjugate heat transfer prediction shows that the stator part is heated up by the main stream gas. This process causes the temperature of the upper part of the stator support to be higher than the gas temperature inside the cavities. Therefore, temperature gradients across the conjugate surfaces may introduce thermal strains at these regions. The lower part of the stator support is away from the main gas path and is at the same temperature level as the surrounding gas.

The static pressure distribution is shown in Figure 6 and the pressure can be seen to remain constant in each inner cavity. The pressure gradient across the cavity is the main mechanism to drive the secondary flow across the passage. The calculated mass fluxes and the gas temperatures through the seals are shown in Table I and are compared with the design data. A prediction without including the conjugate heat transfer for the stator support (Ref. 12) is also shown. As seen, a fair to good agreement is demonstrated and the effects of including the stator support in the temperature prediction are very significant. For example, at path no. 5, the temperature is increased by almost 157 K. Accordingly, the mass fluxes are also affected by the temperature changes.

Stage 2-3 and 3-4 Cavities

Compared to the Stage 1-2 cavities, the Stages 2-3 and 3-4 cavities have a much larger size as well as aspect ratios that are larger in the radial direction, and this alters the flow structures in these cavities. The left side cavities have a higher aspect ratio than the right cavities in both pairs (Figure 1), and this changes the overall shapes of the recirculation patterns in the left and right cavities. For the Stage 2-3 cavities, the cooling flow is introduced at two locations, while for the Stage 3-4 the coolant purge flow is introduced at a point between the interstage labyrinth seals. The labyrinth seal clearances are: 0.3708 and 0.2946 mm to the left and right of the purge injection location in the Stage 2-3 cavities, and 0.1295 and 0.1956 mm for the corresponding locations in the Stage 3-4 cavities. The streamline (Figure 3) patterns in the two left cavities are similar, as are the patterns in the two right cavities. The flow patterns near the rim seals indicate that, at the takeoff condition, none of the rim seals ingests the mainstream gas, and this effect is reflected in the temperatures that are seen in the four cavities (Figure 5), which are much below the main flow path gas temperatures. The temperatures in the right cavities in both the configurations are lower as compared to the left-hand cavities, and one of the reasons for this is that the flow in the right-hand cavities generally has higher velocities. The higher velocities generate a decrease in gas temperatures as well as promote better mixing. In the left-hand cavities the flow is nearly stagnant at the central stationary walls and thus increases the gas temperatures in contact with the walls.

The conjugate heat transfer analyses include the central support walls as well as the rotor support walls. The temperatures in the walls are also shown in Figure 5. In both cases, the region near the stator vanes show the highest temperatures, which decreases rather slowly as one moves radially inward. This decrease reflects the much larger conductivity of the solid material as compared to the gas. These relatively high temperatures will generate thermal strains in these walls and can result in changes in the interstage labyrinth seal clearances and alter the cavity flow fields. Similarly, the rotor support walls also have higher temperatures near the main gas path and the temperatures decrease as one moves radially inward. It is interesting to notice that the temperature in the rotor in between Stages 1-2 and 2-3 cavities decreases much faster than the one in between Stages 2-3 and 3-4. The main reason is that a low coolant flow temperature is specified at the lower left-hand side wall of the first rotor, while the same coolant flow temperature is only specified at the bottom of the second rotor support. The static pressure distributions for Stages 2-3 an 3-4 are shown in Figure 7. As for Stage 1-2, there is very little pressure gradient in each of the four cavities. Most pressure gradients are due to the pressure differences across the pairs of cavities and the higher pressure of the

coolant flow injected from the bottom of the cavities.

The flow rates and gas temperatures through the rim seals are shown in Table 2. The corresponding predicted results from Ref. 12 are also shown in Table 2 for a comparison. In Ref. 12, the Stages 2-3 and 3-4 cavities were computed separately without the inclusion of the rotor supports. Also shown are the calculated static pressure values in the four cavities. The pressure values compare well with the design data. The computed mass flow rates do not correlate as well with the design values, with differences of up to 30% on the Stage 2-3 cavities. In addition, the relative flow splits are not similar: computed results show higher flow rates through the right rim seals while the design data predict the opposite. One of the reasons for the differences may be the location(s) and numbers of coolant injection points; computational grid refinement may also be needed.. Double and a single injection points are assumed for the Stages 2-3 and 3-4 cavities, whereas there probably are multiple leakage paths.

Comparing the results with those of Ref. 12, one can see that coupling solutions and including the rotor supports alter the flow characteristics near the rim seals. For example, the temperature at location B is increased by 78 K. However, the effects on the mass fluxes at the rim seals locations are minimal.

SUMMARY

Flow and conjugate heat transfer computations were performed for multiple disc cavities in the turbine section of the Allison T56/501D engine using an advanced CFD code, SCISEAL. The following remarks can be made based on the results:

1. The predicted results for the mass flows and gas temperatures at rim and labyrinth seals show fair agreement with Allison T56/501D engine design calculations. The agreement is better in the Stage 1-2 cavities with better defined purge flow injection locations. Mass flow rates in the stage 2-3 and 3-4 cavities show higher differences.
2. Both the stator and rotor support walls are included in the heat transfer calculation. The conjugate heat transfer analysis shows that, due to contact with the hot main stream gas, these support walls are at higher temperatures than the surrounding gas in the cavities. This type of information can be useful in the predictions of the thermal strains in the solid portions, which may affect the interstage seal clearances, cavity flow fields and longevity of the disc.
3. The inclusion of the rotors supports in the calculation shows that the flow temperatures near the rim seals are further increased (compared to a prediction without including the rotor supports) due to the contribution of the heat transfer in the rotor supports.

With the available flow information, calculations can be done in the future to assess the effects of thermal strains on the seal flows. Future efforts may also include coupling of the cavity flows with the main path flow and the time dependent effects due to the blade wakes in the main path flow.

ACKNOWLEDGEMENTS

This work was supported by NASA Lewis Research Center under the contract NAS3-27392. This support is greatly appreciated.

REFERENCES

Owen, J.M., and Pincombe, J.R., "Velocity Measurements Inside a Rotating Cylindrical Cavity with a Radial Outflow of Fluid," *J. Fluid Mechanics*, Vol. 99, p. 111, 1980.

Owen, J.M., Pincombe, J.R., and Rogers, R.H., "Source-Sink Flow Inside a Rotating Cylindrical Cavity," *J. Fluid Mechanics*, Vol. 155, pp. 233-265, 1985.

Phadke, U.P., and Owen, J.M., "An Investigation for an Air-cooled Shrouded Rotating Disk System with Radial Clearance Seals," *Trans. ASME, J. of Engineering for Gas Turbine and Power*, Vol. 110, pp. 78-85, 1988.

Hasser, F., Jack, J., and McGreehan, W., "Windage Rise and Flowpath Gas Ingestion in Turbine Rim Cavities," *Trans. ASME, J. of Engineering for Gas Turbine and Power*, Vol. 110, pp. 78-85, 1988.

Chew, J.W., "Predictions of Flow in Rotating Disk Systems Using the k-ε Turbulence Model," ASME-88-GT-229, ASME Gas Turbine and Aeroengine Expo, Amsterdam, The Netherlands, 1988.

Chew, J.W., "A Theoretical Study of Ingress for Shrouded Rotating Disc Systems with Radial Outflow," ASME-89-GT-178, ASME Gas Turbine and Aeroengine Expo, Toronto, Canada, 1989.

Ko, S.H., and Rhode, D.L., "Thermal Details in a Rotor-Stator Cavity at Engine Conditions with a Mainstream," ASME-91-GT-275, ASME Gas Turbine and Aeroengine Expo, Orlando, FL, 1991.

Athavale, M.M., Przekwas, A.J., and Hendricks, R.C., "A Numerical Study of the Flow Field in Enclosed Turbine Disk Cavities in Gas Turbine Engines," 4th International Symposium on Transport Phenomena and Dynamics of Rotating Machinery (ISROMAC-4), Honolulu, HI, 1992.

Hendricks, R.C., Griffin, T.A., Kline, T.R., Csavina, K.R., Pancholi, A., and Sood, D., "Relative Performance Comparison between Baseline Labyrinth and Dual-Brush Compressor Discharge seal in a T-700 Engine Test," Presented at the 39th International Gas Turbine and Aeroengine Conference, Netherlands, 1994.

Virr, G.P., Chew, J.W., and Coupland, J., "Application of Computational Fluid Dynamics to Turbine Disk Cavities," *Trans. ASME, J. of Turbomachinery*, Vol. 116, pp. 701-708, 1994.

Athavale, M.M., Przekwas, A.J., Hendricks, R.C., and Steinetz, B.M., "Numerical Analysis of Intra-Cavity and Power-Stream Flow Interaction in Multiple Gas-Turbine Disk-Cavities," ASME-95-GT-325, presented at the ASME Gas Turbine Congress and Exposition, Houston, TX, 1995.

Athavale, M.M., Ho, Y.-H., Forry, J.M., Munson, J.H., Hendricks, R.C., and Steinetz, B.M., "Simulation of Secondary Flow in Gas Turbine Disc Cavities and Interaction with the Main Flow Path," AIAA-95-2620, Presented at the 31st AIAA/ASME/SAE/ASEE Join Propulsion Conference, San Diego, CA, July 10-12, 1995.

Athavale, M.M., Przekwas, A.J., Hendricks, R.C., and Liang, A., "SCISEAL - A Three-Dimensional CFD Code for Accurate Analyses of Fluid Flows and Forces in Seals," Presented at the Conference on Advances Earth-To-Orbit Technology, NASA MSFC, Huntsville, AL, May 1994.

Przekwas, A.J., Athavale, M.M., and Hendricks, R.C., "Progress in Advanced Modeling of Turbine Engine Seal Flows," AIAA Paper 94-2803, 1994.

Athavale, M.M., Przekwas, A.J., J.H., Hendricks, R.C., and Steinetz, B.M., "Numerical Analysis of Intra-Cavity and Power-Stream Flow Interaction in Multiple Gas-Turbine Disk-Cavities," ASME Paper 95-GT-325, 1995.

Table 1. Comparison between the Design Data and the Prediction for Stage 1-2 Cavities (see Figure 1 for path no. notation).

Path No.	Design		Prediction (include conjugate heat transfer for solid parts)		Previous Prediction (without conjugate heat transfer for Stage 1-2 and rotors , Ref. 12)	
	Maseflow(kg/s)	Temperature (K)	Massflow(kg/s)	Temperature (K)	Massflow (kg/s)	Temperature (K)
4	0.1129	843	0.1284	870	0.1397	829
5	0.0186	843	0.0249	984	0.0136	827
6	0.0449	843	0.0481	893	0.0431	866

Table 2 Comparison between the Design Data and the Prediction for Stages 2-3 and 3-4 Cavities (see Figure 1 for locations notation).

Locations	Design			Prediction (include conjugate heat transfer for all solid parts)			Previous Prediction (without conjugate heat transfer for Stage 1-2 and rotors, Ref.12)		
	Mass (kg/s)	Pressure (Pa)*x10^5	Temperature (K)	Mass (kg/s)	Pressure (Pa)*x10^5	Temperature (K)	Mass (kg/s)	Pressure (Pa)*x10^5	Temperature (K)
A	0.0567	3.309	741	0.0390	3.282	790	0.0376	3.275	786
B	0.0376	2.137	696	0.0522	2.089	794	0.0540	2.066	716
C	0.0340	1.724	705	0.0249	1.682	769	0.0240	1.689	700
D	0.0209	1.103	703	0.0263	1.082	732	0.0272	1.069	666

* Values at the center of the cavities.

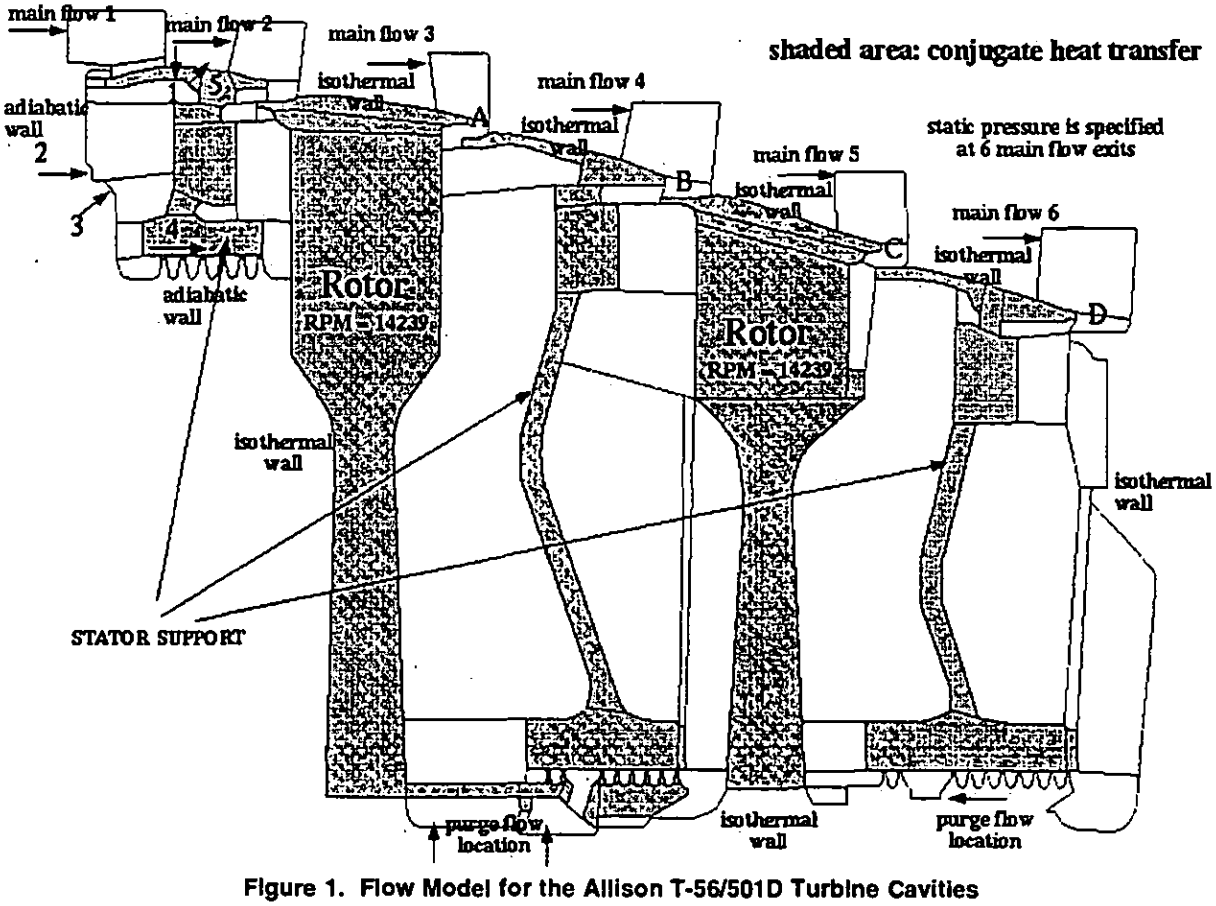

Figure 1. Flow Model for the Allison T-56/501D Turbine Cavities

Stream Function

Contour Levels

2 −6.6E−2
4 −4.6E−2
6 −2.6E−2
8 −6.0E−3
10 1.4E−2
12 3.4E−2

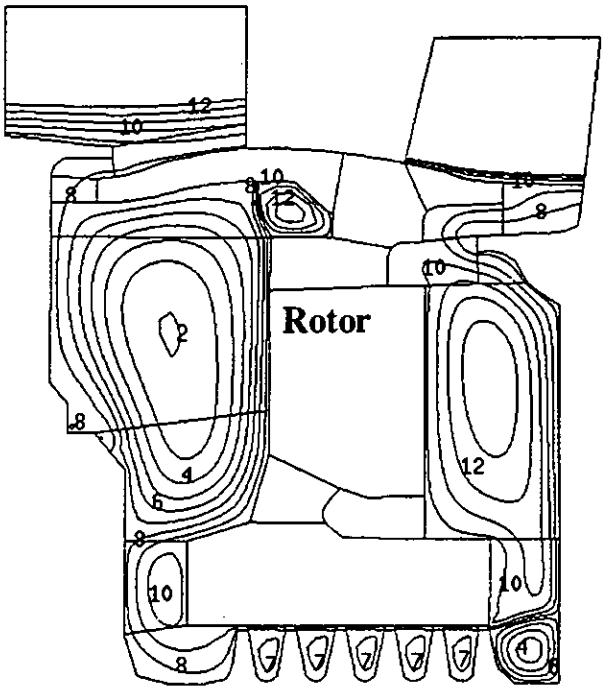

Figure 2 Stream Function Distribution inside the Stage 1–2 Cavities.

Stream Function

Contour Levels

2 −3.15E−2
4 −2.45E−2
6 −1.75E−2
8 −1.05E−3
10 −3.50E−3
12 3.50E−3

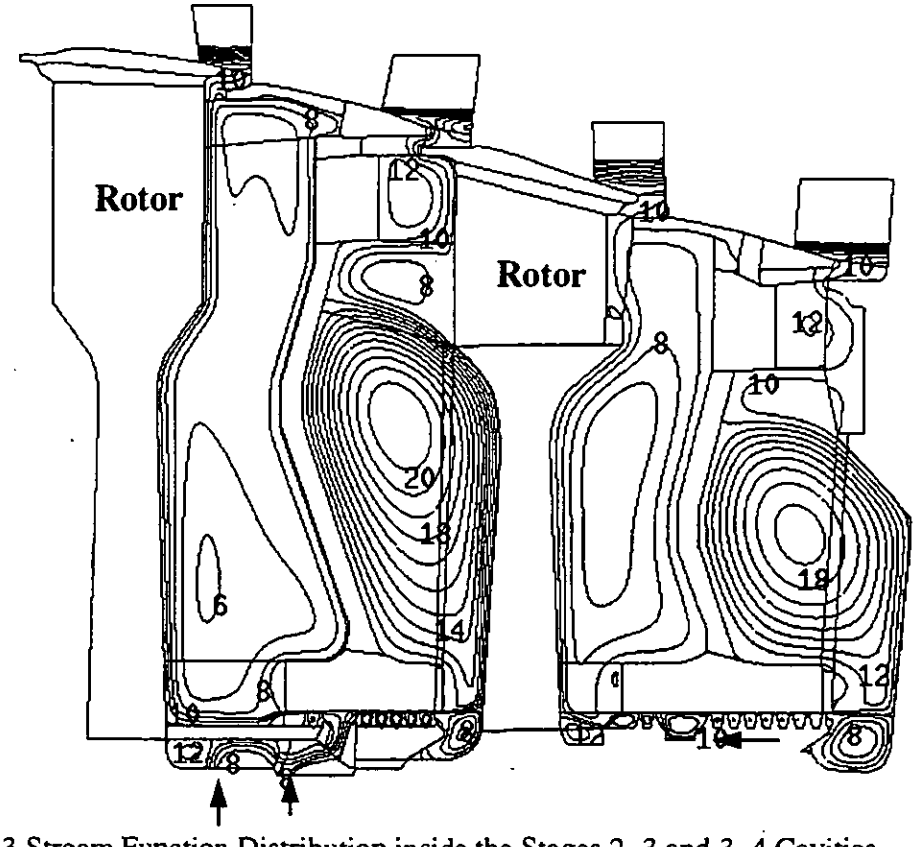

Figure 3 Stream Function Distribution inside the Stages 2–3 and 3–4 Cavities.

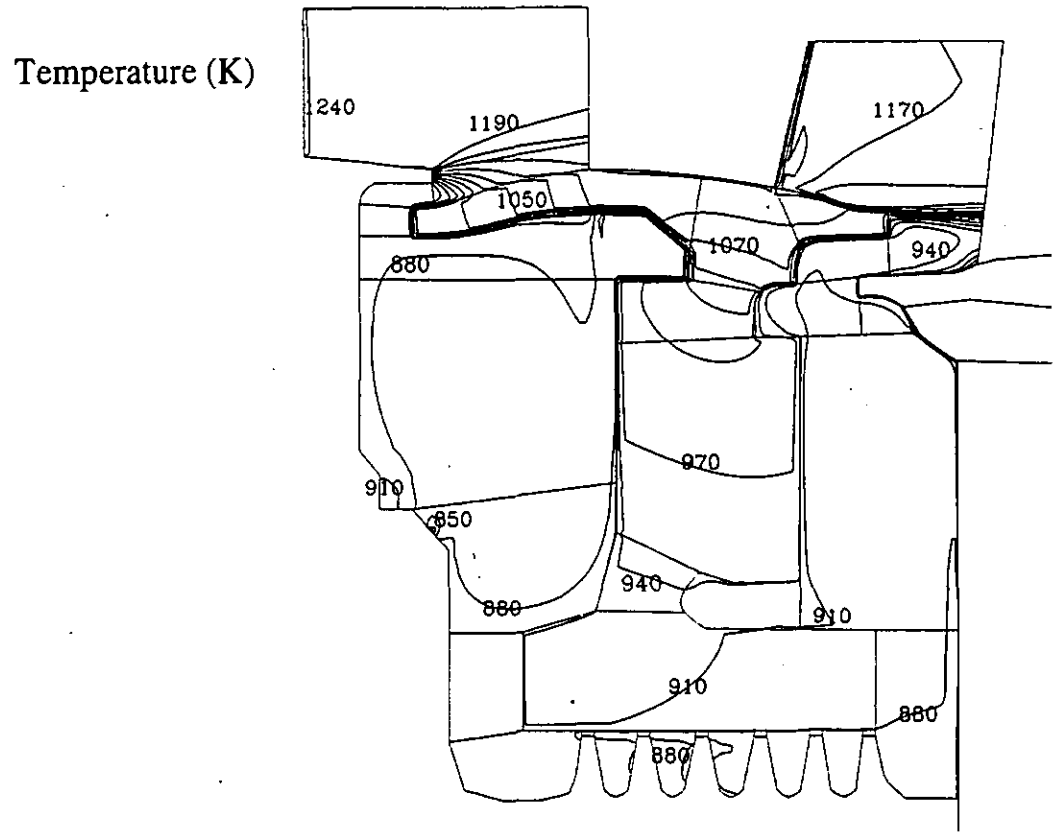

Figure 4 Static Temperature Distribution inside the Stage 1–2 Cavities and the Central Support Wall.

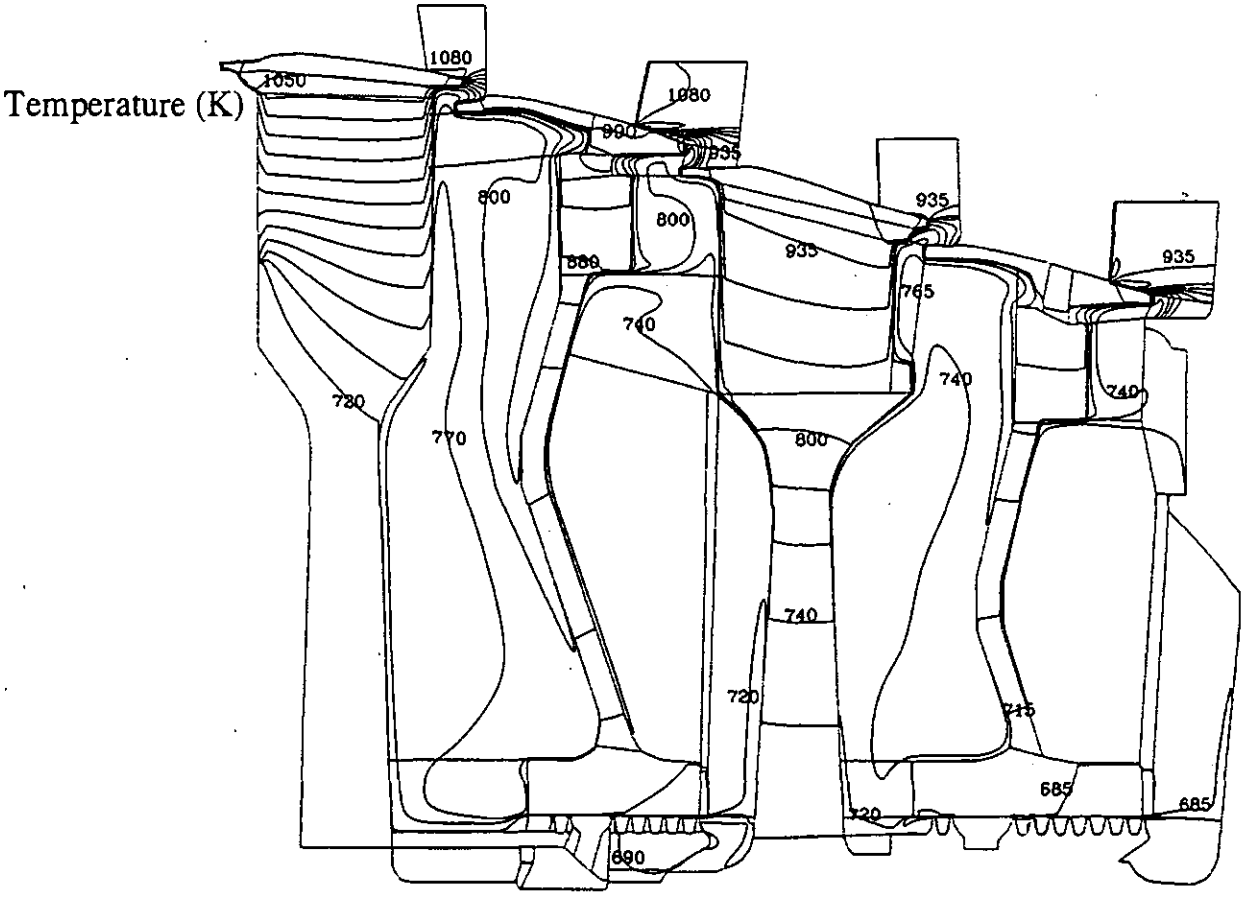

Figure 5 Static Temperature Distribution inside the Stages 2–3 and 3–4 Cavities , the Central Support Walls and the Rotors Support Walls.

Static Pressure (Pa)

Contour Levels

2	3.4E+5
4	3.6E+5
6	3.8E+5
8	4.0E+5
10	4.2E+5
12	4.4E+5
14	4.6E+5
16	4.8E+5
18	5.0E+5
28	6.0E+5

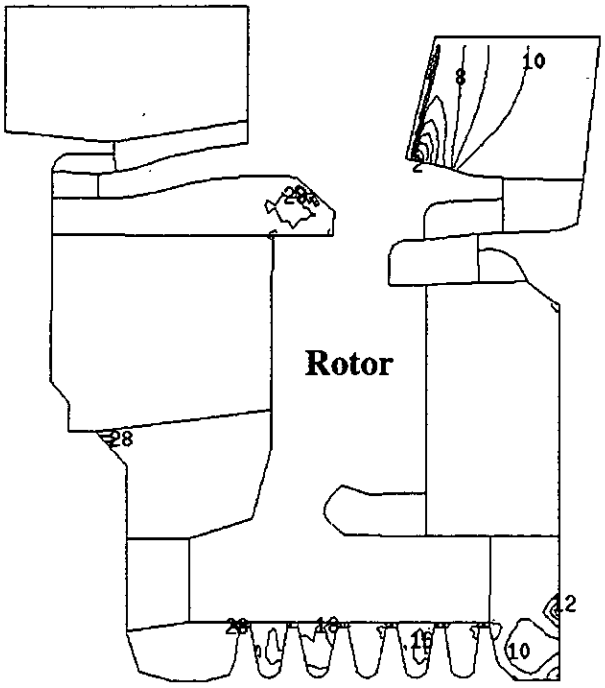

Figure 6 Static Pressure Distribution inside the Stage 1–2 Cavities.

Static Pressure (Pa)

Contour Levels

2	9.0E+4
4	1.3E+4
6	1.7E+4
8	2.1E+5
10	2.5E+5
12	2.9E+5
14	3.3E+5

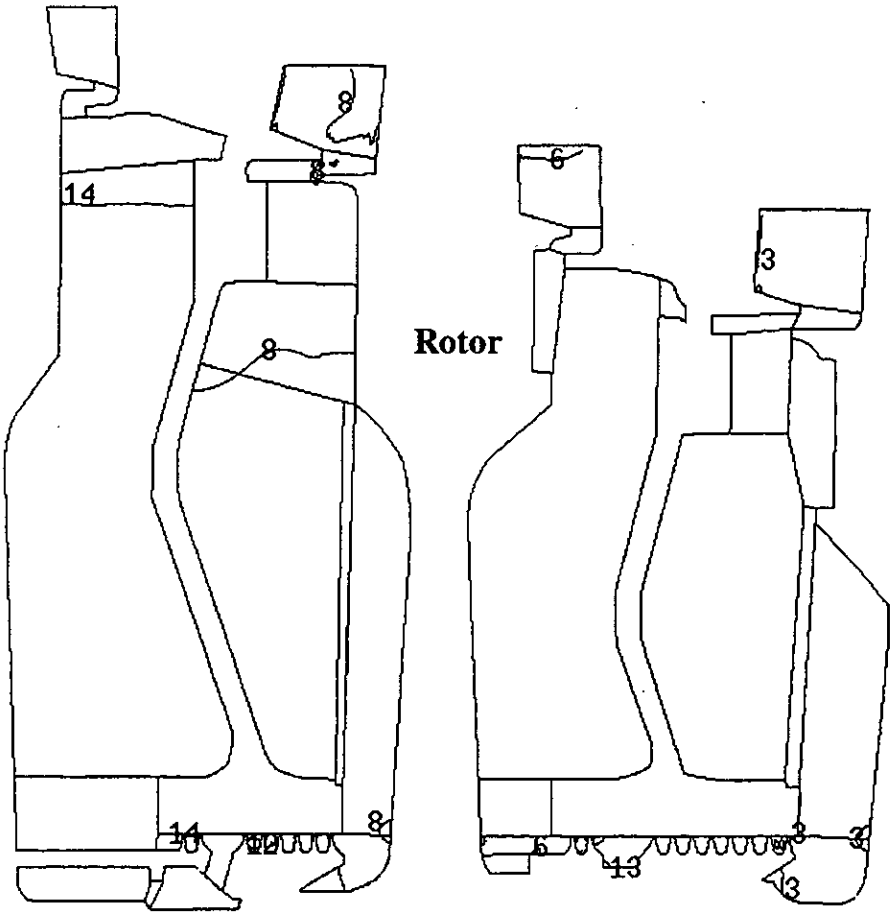

Figure 7 Static Pressure Distribution inside the Stages 2–3 and 3–4 Cavities.